The following supplement accompanies the article

Modeling aggregate dynamics of transparent exopolymer particles (TEP) and their interactions with a pelagic food web

Temel Oguz*

*Corresponding author: temeloguz@gmail.com

Marine Ecology Progress Series 582: 15–31 (2017)

Supplement

Observed characteristics of the Marmara Sea

The Marmara Sea is a semi-enclosed basin linked to the Black and Aegean Seas by the Strait of Istanbul (Bosphorus) and the Strait of Canakkale (Dardanelles). It possesses a two-layer stratified system that is characterized by roughly 20 m thick low salinity (24 ± 3 psu) upper layer water mass of the Black Sea origin overlying a more saline (~38.5 psu) Mediterranean water mass that attains a temporally uniform temperature of ~ 14.5^{o}C. The upper layer with relatively low temperature of 6-7^{o}C and high salinity of 25-27 psu may deepen to 25m during winter whereas the upper 15m layer may warm up to 26^{o}C and freshen to 21 psu during summer (Fig. S1 and Fig. S2). The distinctly different upper and lower layer water masses are separated by the 15-20 m thick interface having a strong density contrast of ~5-8 kg m^{-3}.

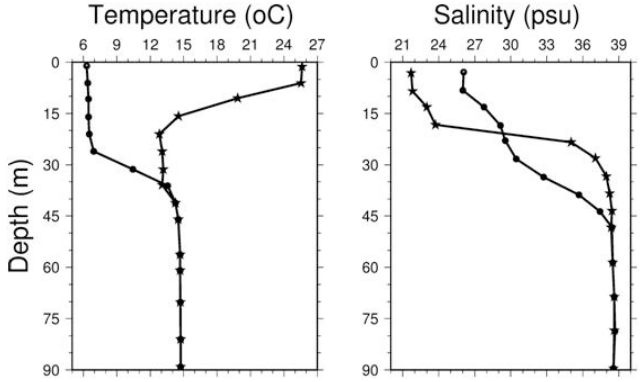

Fig. S1. Temperature and salinity profiles in the southeastern basin of the Marmara Sea during January (●) and July (*). Re-plotted from Yılmaz et al. (2005) based on the 2001-2002 monthly measurements.

Whereas the strong and narrow permanent pycnocline limits vertical exchange of biogeochemical properties, the upper layer receives nutrients from the Black Sea and from the domestic, industrial, and agricultural sources. Nitrate is the main limiting nutrient that increases from values less than 0.5 mmol m^{-3} near the surface to around 10 ± 1 mmol m^{-3} below the pycnocline over the year (Fig. S3). The lower layer is persistently hypoxic with oxygen concentrations around 50 ± 20 μM due to intense oxygen consumption during remineralization of particulate matter, whereas oxygen concentration of the upper 20m may be as high as 300 μM in response to the air-sea flux and oxygen generation by photosynthesis (Fig. S3). The dissolved oxygen flux incoming from the Aegean Sea by the lower layer flow ventilates its sub-pycnocline water column to prevent the development of unoxic conditions.

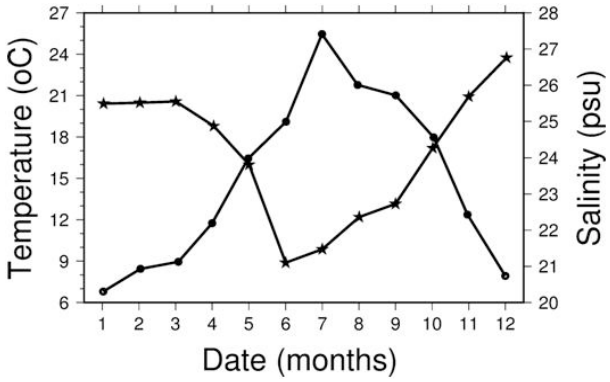

Fig. S2. Monthly variations of sea surface temperature (●) and salinity (*) in the southeastern basin of the Marmara Sea based on the 2001-2002 measurements. Re-plotted from Yılmaz et al. (2005).

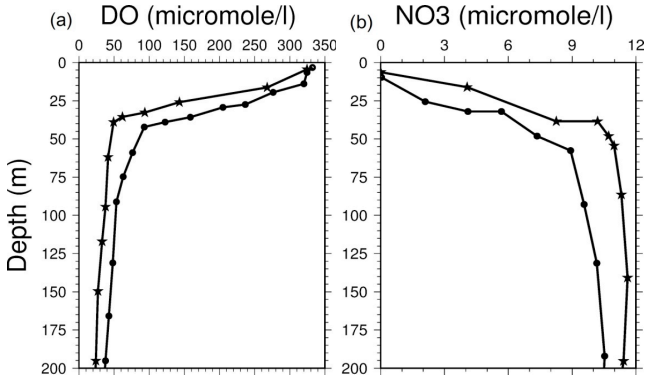

Fig. S3. Dissolved oxygen and nitrate concentration profiles in the southeastern basin of the Marmara Sea during March 2015 (●) and July 2013 (*). Re-plotted from Ediger et al. (2016).

The satellite ocean color data possess relatively high annual mean primary production up to ~ 600 mg C m^{-2} yr^{-1} in different parts of the basin (Chassot et al., 2007) and even higher at coastal regions. Several time series measurements (Yilmaz et al., 2005; Isinibilir et al., 2008; Isinibilir, 2012) documented successive blooms of phytoplankton during autumn-winter as inferred by surface chlorophyll concentations retrieved by the MODIS satellite data in Fig. S4. The winter phytoplankton bloom is followed by the biomass increase of mesozooplankton in winter-spring, and of red tide species heterotrophic dinoflagelate *Noctiluca scintillans* in late spring-early summer. The zooplankton community structure is dominated by *Noctiluca* having abundance almost an order of magnitude higher than fodder zooplankton (copepods and cladocerans) as shown by Fig. S5. The jellfish/ctenophore species dominated by the gelatinous ctenophore *Mnemiopsis leidyi* undergo population rise in the late summer-autumn and the population drops abruptly by the end of autumn due to the predation pressure exerted by its predator *Beroe ovata* (Isinibilir, 2012). These data sets are used to tune the model parameters to reproduce the observed characteristic features of the food web structure.

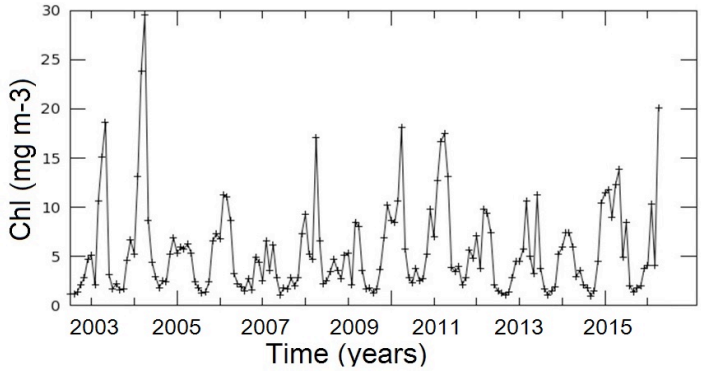

Fig. S4. Monthly variations of surface chlorophyll concentration averaged over region between 27^{o} and 29^{o}E longitudes and 40^{o} and 41^{o}N latitudes during 2002-2016. The data are provided by 4km resolution MODIS-Aqua satellite sensor measurements.

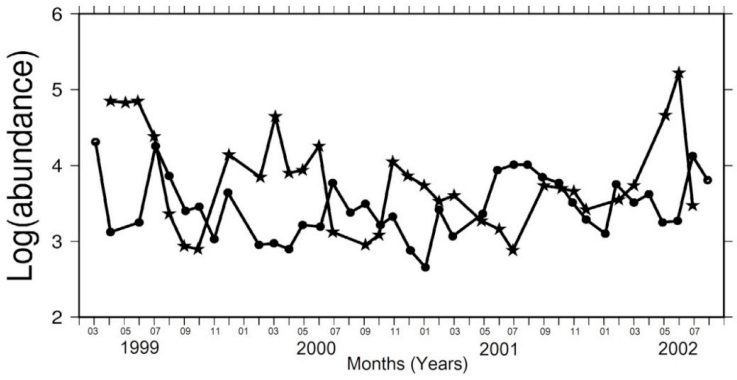

Fig. S5. Monthly variations of sea surface zooplankton (●) and *Noctiluca* (*) abundance in the south-eastern basin of the Marmara Sea based on 2001-2002 measurements. Re-plotted from Yılmaz et al. (2005).

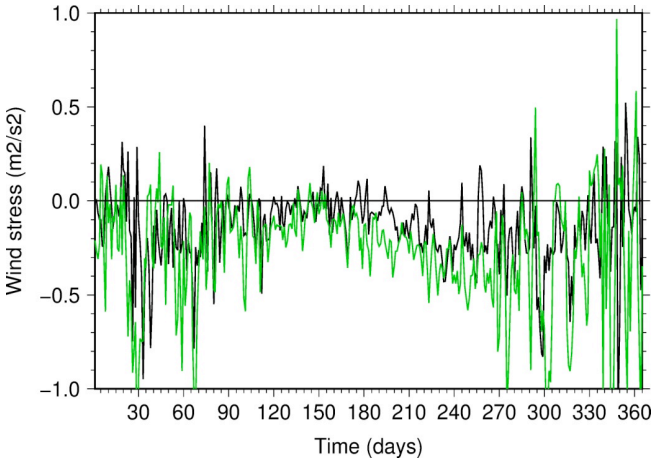

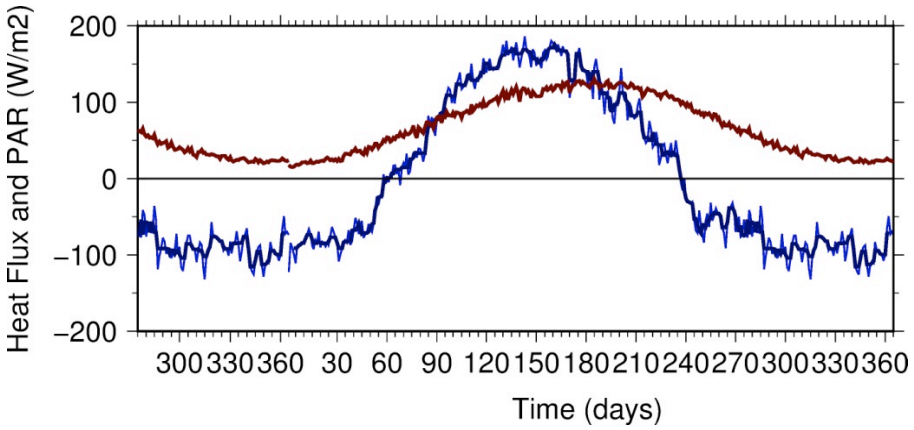

Fig. S6. The daily changes of the eastward (black) and northward (green) components of wind stress vector (to be multiplied by 0.0001 m^2 s^{-2}), and the total heat flux (blue) and photosynthetically available radiation (PAR) (red) in W m^{-2}). The wind stress variations indicate domination of the northeasterlies over the year. Cooling is indicated by negative values of the total heat flux.

Description of the source-sink terms for the biogeochemical model equations

The rate of change of each of the state variables of the biogeochemical model is expressed by

$$\frac{\partial X}{\partial t} + \nabla\left(\vec{u} \cdot X\right) = F_X + R(X) \qquad \text{(S1)}$$

where X denotes the state variable, $\boldsymbol{u}$ is the three dimensional fluid velocity, F_X denotes the sum of horizontal and vertical diffusion terms represented similar to those in the circulation model, and $R(X)$ denotes the collection of biological source-sink terms that are described below together with the list of parameters and their values in Tables S1-S4.

S1. The autotrophs

The biological source-sink terms in the phytoplankton equation (Eq. S2) include, respectively, the phytoplankton growth (primary production) that is reduced by exudation, overall limitation function (Eq. S2a), grazing by different zooplankton groups, and physiological mortality. Primary production is limited by temperature (only for the diatom group; Eq. S2f), and the availability of light (Eq. S2b,c), nutrients (Eq. S2d,e). Dissolved oxygen concentration also inhibits phytoplankton growth within hypoxic waters of the lower layer (Eq. S2g). The total nitrogen limitation is expressed by the sum of ammonium and nitrate limitations $f_k(N_a)$ and $f_k(N_n)$ defined by Eq. S2e. The role of nitrate limitation weakens in the presence of ammonium and no silicate limitation is imposed for the growth of diatoms due to the relatively high silicate availability in the system.

The temperature limitation (Eq. S2f) is imposed for diatoms only to promote their preferential growth at low temperatures below 12°C. The value of Q_{10} parameter is set to 2.0. The light limitation function (Eq. S2b) is represented by the hyperbolic tangent function modified by adding a weak photoinhibition term (Bisset et al., 1999). $I(z,t)$ denotes the photosynthetically available irradiance (PAR) with the surface value (I_s) corresponding to half of the incoming solar

radiation. The parameter a_k in Eq. S2b defines the initial slope of the growth versus light relationship at low light values. It represents a simplified form of more general expression in terms of the maximum growth rate (a_k/σ_k). The exponential photoinhibition term is applied only to the diatom group so that the small phytoplankton group comprising pico- and nanophytoplankton cells allows more favorable growth at low nutrient–high light and high temperature conditions contrary to the larger size groups (diatoms and dinoflagellates). This is achieved by setting the initial slope of light limitation curve for the diatom group to a higher value, specifying relatively high values for the half saturation constants of nitrate and ammonium uptakes for diatom and assigning a higher mortality rate for the smaller size group. The relatively high light attenuation coefficient (greater than 0.1 m^{-1}) limits the vertical extent of the euphotic zone to upper 30 m at most. The decay parameter α_k inhibits light under relatively high irradiance conditions (e.g. $I_s > 80\ Wm^{-2}$).

$$R(P_X) = (1-\kappa)\cdot\sigma_k\cdot\Psi_X\cdot P_X - \sum_k G_k(P_X)\cdot Z_k - m_{PX}\cdot P_X \quad \text{(S2)}$$

$$\Psi_X = f_X(N_n, N_a)\cdot f_X(I)\cdot f_X(T)\cdot f_X(DO) \quad \text{(S2a)}$$

$$f_X(I) = \tanh[\alpha_X\cdot I]\cdot e^{-\beta_X(I-I_{0X})} \quad \text{(S2b)}$$

$$I = I_S\cdot\exp\left\{-\mathrm{k_w z} - k_b\cdot\int_0^z(\mathrm{P_D}+\mathrm{P_F}+\mathrm{P_S}+\mathrm{D_n})\cdot dz\right\} \quad \text{(S2c)}$$

$$f_X(N_n, N_a) = f_X(N_n) + f_X(N_a) \quad \text{(S2d)}$$

$$f_X(N_a) = \left[\frac{N_a}{K_{AX}+N_a}\right] \qquad and\ f_X(N_n) = [1-f_X(N_a)]\cdot\left[\frac{N_n}{K_{NX}+N_n}\right] \quad \text{(S2e)}$$

$$f_D(T) = Q_{10}^{(12-T)/12} \quad \text{(S2f)}$$

$$f(DO) = \left[\frac{DO}{250\mu M + DO}\right] for\ DO < 150\mu M, \qquad f(DO) = 1\ \ otherwise \quad \text{(S2g)}$$

Bacteria biomass is subject to temporal changes (Eq. S3) due to DON and ammonium uptakes (Eqs. S4a,b), grazing by heterotrophic dinoflagellate species *Noctiluca* and microzooplankton, losses due to mortality and excretion. The sum of DON and ammonium uptake is assumed to always limit the bacterial growth more strongly than the DOC uptake, as a simplified case of the formulation provided by Anderson and Williams (1998).

$$R(Ba) = G_B(N_a) + G_B(DON_L) - G_S(B)Z_S - G_N(Ba)Z_N - \mu_B B - m_B Ba \quad \text{(S3)}$$

$$G_B(N_a) = g_{B\max}\cdot f_B(DO)\cdot Ba\cdot\left[\frac{N_a}{K_a+N_a}\right] \quad \text{(S4a)}$$

$$G_B(DON_L) = g_{B\max}\cdot f_B(DO)\cdot Ba\cdot\left[\frac{DON_L}{K_L+DON_L}\right] \quad \text{(S4b)}$$

S2. The heterotrophs and carnivores

The biomass changes in the zooplankton groups and the small pelagic fish are controlled, respectively, by ingestion, predation, excretion, and mortality according to

$$R(Z_X) = \gamma_Z \left[\sum_k G_X(P_k) \right] Z_X - \sum_k G_k(Z_X) Z_k - \mu_X Z_X - m_{ZX} Z_X^2 \qquad \text{(S5)}$$

Diatom and dinoflagellate, *Noctiluca,* microzooplankton together with the particulate organic nitrogen contribute to the mesozooplankton feeding (Table S1). The diet of *Noctiluca* is similar, but with a better competitive advantage (Table S1). The microzoo- and mesozooplankton groups constitute main diets for the jellyfish and planktivore fish at different proportions. *Noctiluca* and planktivore fish larvae may also contribute to the jellyfish diet at relatively small proportions. Zooplankton grazing is defined by the Michaelis–Menten (the so-called Holling type II) functional form for kth predator on ith prey (Eq. S6a) in terms of the maximum rate g_k, the temperature limitation function $f_k(T)$ and the food capture efficiency coefficients $b_{k,i}$ expressed based on prey feeding selectivity (Eq. S6b). This parameterization however ignores taxonomic preferences of zooplankton groups to actively select or reject individual prey items. Zooplankton growth is suppressed under low oxygen conditions (Eq. S2g). The growth rates of mesozooplankton and *Noctiluca* are controlled by temperature (Eq. S6c,d) to support the biomass increase or decrease during specific periods of the year, whereas the growth rate of gelatinous carnivore species is made time dependent to parameterize its population growth during late summer-autumn (Eq. S6e). The temperature dependence of the mortality rate of the gelatinous group (Eq. S6f) maintains its low biomass throughout the year except its peak in August - October period that also partially parameterize the predation pressure exerted by the predator species *Beroe ovata*. The excretion rates are expressed by the hyperbolic function depending on the biomass changes (Eq. S6g). *Noctiluca* attains higher excretion rate with respect to the other zooplankton groups in consistent with the observations (Table S3). The planktivorous fish compartment in the model serves mainly as a food source for the jellyfish rather than simulating its observed stock changes. Its lower growth rate and relatively high fishing mortality provide its competitive disadvantage with respect to the jellyfish.

$$G_j(X_i) = g_j \cdot f_j(T) \cdot f(DO) \cdot \frac{b_{j,i} \cdot X_i}{K_j + \left[\sum_i b_{j,i} \cdot X_i \right]} \qquad \text{(S6a)}$$

$$b_{j,i} = \frac{a_{j,i} \cdot X_i}{\sum_i a_{j,i} \cdot X_i} \qquad \text{(S6b)}$$

$$f_{ZL}(T) = Q_{10}^{(T-12)/6} \qquad f_{ZL}(T) = \max\left(f_{ZL}(T), 2\right) \qquad \text{(S6c)}$$

$$f_{ZN}(T) = Q_{10}^{(T-13)/6} \qquad \text{(S6d)}$$

$$g_{ZG} = \begin{cases} 0.1 g_0 & for \quad day < 190 \\ 0.1 g_0 + 0.02 * (day - 190) * g_0 & for \quad 190 \le day \le 240 \\ 1.1 g_0 \cdot Q_{10}^{(T-21)/3} & for \quad day > 240 \end{cases} \qquad \text{(S6e)}$$

$$m_G = m_{0,G} \cdot \left(1 + \frac{8^o C}{T}\right) \tag{S6f}$$

$$\mu_X = \mu_{\max,X} \frac{X}{K_{eX} + X} \tag{S6g}$$

S3. Particulate organic nitrogen

According to Eq. S7, the particulate organic nitrogen pool is governed by a fraction of the unassimilated food (the first term on the right hand side) and phytoplankton and zooplankton fecal pellets (the terms within the first square brackets) and its consumption by *Noctiluca* and mesozooplankton (the terms within the second square brackets), an oxygen dependent remineralization), and sinking to deeper levels with a sinking speed depending on its concentration. The grazing, remineralization and sinking terms are expressed by Eqs. S8a-c. As in the case of Druon et al. (2010), 70% of particulate organic nitrogen is assumed to decompose directly into ammonium. It represents highly labile fraction of DON having turnover rates on the order of several days. The rest contributes to the DON source given by Eq. A14 in Appendix together with the labile and semi-labile forms of dissolved organic nitrogen equation in Eq. A16.

$$\begin{aligned} R(D_n) = (1-\gamma_Z)\cdot\beta\cdot Graz + \left[\sum_X m_{P,X} P_X + \sum_X m_{Z,X} Z_X^2\right] \\ -\gamma_Z \cdot \left[G_N(D_n) Z_N + G_L(D_n) Z_L\right] - \varepsilon_n \cdot D_n - \frac{\partial (w_D \cdot D)}{\partial z} \end{aligned} \tag{S7}$$

$$Graz = \sum_X \left[\sum_k G_X(P_k) + \sum_k G_X(Z_k)\right] \cdot Z_k \tag{S8a}$$

$$\varepsilon_n = \varepsilon_{n0} \cdot f_\varepsilon(DO); f_\varepsilon(DO) = \frac{DO}{150\mu M + DO}; f_\varepsilon(DO) = \min\left[f_\varepsilon(DO), 0.25\right] \tag{S8b}$$

$$w_D = w_{D\max}\left[1 + \frac{D_n}{0.5 + D_n}\right] \tag{S8c}$$

S4. Dissolved inorganic nitrogen and oxygen

The ammonium equation (Eq. S9) comprises its uptake during the primary and bacterial productions (Eqs. S2e & S4a), productions due to the decomposition of particulate organic nitrogen, zooplankton excretion, and its conversion to nitrate (i.e. the nitrification) using a light dependent nitrification rate.

$$R(N_a) = -\sum_k f_k(N_a) - G_B(N_a) + \sum_k \mu_{zk} \cdot Z_k - r_a \cdot \left(\frac{I_n}{I_n + I}\right) \cdot N_a + \lambda \cdot \varepsilon_n \cdot D_n \tag{S9}$$

The sinks in the nitrate equation (Eq. S10) arise from the losses due to uptake and oxidation processes under low oxygen conditions whereas the nitrification process forms the internal source. The nitrate equation also includes the nudging term to restore its lower layer concentrations (below 40m depth) to the climatologically-derived mean values with the restoring time scale of τ=50 days. This nudging term parameterizes the complex biogeochemical processes within the lower layer that are unresolved in the context of the present study.

$$R(N_n) = r_a \cdot \left(\frac{I_n}{I_n + I} \right) \cdot N_a - \sum_k f_k(N_n) - r_n \cdot N_n^2 + \frac{1}{\tau}(N_{n,c\lim} - N_n) \quad \text{(S10)}$$

Dissolved oxygen concentration increases with photosynthesis, reduces due to its consumption by the excretion, remineralization, oxidation processes (Eq. S11). Its concentrations below 40m depth are restored to their climatological values to maintain the hypoxic conditions via lateral oxygen supply from the Aegean Sea. The restoring time scale is taken as τ=50 days.

$$\begin{aligned} R(DO) = 8.125 \cdot \left[\sum_k \Psi_k \cdot P_k \right] - 6.625 \cdot \left[\varepsilon_n \cdot D_n + \sum_k \mu_{zk} \cdot Z_k \right] \\ - 2r_a \cdot \left(\frac{20}{20 + I} \right) \cdot N_a + \frac{1}{\tau}(DO_{c\lim} - DO) \end{aligned} \quad \text{(S11)}$$

The air-sea exchanges of surface dissolved oxygen concentration is given by

$$K_v \frac{\partial DO}{\partial z} = -V_p \cdot [DO_{sat} - DO(z=0)] \quad \text{(S12)}$$

where K_v is the vertical diffusivity, DO_{sat} represents the oxygen saturation concentration computed according to the *UNESCO formula* (1996), DO(z=0) is the oxygen concentration at the surface computed by the model, and V_p is the gas transfer velocity computed according to the relation given by Wanninkhof (1992).

References

Anderson TR, Williams B (1998) Modelling the seasonal cycle of dissolved organic carbon at Station E1 in the English Channel. Estuar Coast Shelf Sci 46: 93−109

Bissett WP,. Walsh JJ, Dieterle DA, Carter KL (1999) Carbon cycling in the upper waters of the Sargasso Sea: I. Numerical simulation of differential carbon and nitrogen fluxes. Deep-Sea Research I 46: 205–269

Chassot E, Mélin F, Le Pape O, Gascuel D (2007) Bottom-up control regulates fisheries production at the scale of ecoregions in European seas. Mar Ecol Prog Ser 343: 45–55

Druon JN, Mannino A, Signorini S, McClain C, Friedrichs M, Wilkin J, Fennel K (2010) Modeling the dynamics and export of dissolved organic matter in the Northeastern U.S. continental shelf. Estuarine, Coastal and Shelf Science 88: 488-507

Ediger D, Beken Ç, Yuksek A, Tugrul S (2016) Eutrophication in the Sea of Marmara. In: Özsoy, E, Ça¡gatay MN, Balkis N, Balkis N, Öztürk B (eds) The Sea of Marmara; marine biodiversity, fisheries, conservation and governance. Publication No. 42. Turkish Marine Research Foundation (TUDAV), Istanbul, p 723−736

Isinibilir M (2012) The seasonal occurrence and abundance of gelatinous macrozooplankton in Izmit Bay (the northeastern Marmara Sea). J Black Sea Mediterr Environ 18: 155−176

UNESCO (1996) Progress on oceanographic tables and standards 1983-1986: work and recommendations of the UNESCO/SCOR/ICES/IAPSO Joint Panel, Tech. Pap. Mar. Sci. 50, p. 50.

Wanninkhof R (1992) Relationship between wind-speed and gas-exchange over the ocean. Journal of Geophysical Research (Oceans) 97(C5): 7373–7382.

Table S1. Food preference coefficients of the predator groups on the prey groups.

Prey type	Microzoo	Mesozoo	Gelatinous	*Noctiluca*	*Fish*
Diatom	--	1.0	--	1.0	--
Dinoflagel	--	0.5		1.0	--
Small Phyto	1.0	--	--	--	--
Microzoo	--	0.5	0.2	0.5	0.5
Mesozoo	--	--	1.0	--	1.0
Noctiluca	--	0.5	0.2	--	--
Detritus	--	0.5	0.5	0.5	--
Bacteria	0.8	--	--	--	--
Fish	--	--	0.25	--	--

Table S2. Parameters of the phytoplankton groups

Parameter	Definition	Unit	Diatom	Dinoflagellat	Small phyto
σ_{Pi}	Maximum growth rate	d^{-1}	1.1	1.3	1.5
K_{Ni}	Half saturation constant for nitrate uptake	mmol m^{-3}	0.4	0.35	0.3
K_{Ai}	Half saturation constant for ammonium uptake	mmol m^{-3}	0.3	0.25	0.2
m_{Pi}	Mortality rate	d^{-1}	0.05	0.06	0.06
a_k	Initial slope of PI curve	$(Wm^{-2})^{-1}$	0.08	0.065	0.05
$_k$	Light attenuation constant	$(Wm^{-2})^{-1}$	0.02	0.015	0.01
I_{0k}	Limiting value of light attenuation	W m^{-2}	50	55	60

Table S3. Parameters of the zoooplankton groups

Parameter	Definition	Unit	Micro zoo	Mesozoo	Gelatinous	Noctiluca	Bacteria
r_{Zi}	Maximum growth rate	d^{-1}	1.0	0.4	0.5	0.6	1.0
K_Z	Grazing half saturation constant	mmol m^{-3}	0.5	0.7	0.6	0.45	0.45
m_{Zi}	Mortality rate	d^{-1}	0.07	0.1	0.01	0.1	0.04
μ_{Zi}	Excretion rate	d^{-1}	0.04	0.05	0.05	0.1	0.03

Table S4. Additional parameter values of the biogeochemical model

Parameter	Definition	Unit	Value
k_w	Phytoplankton exctinction coefficient for clear water conditions	m^{-1}	0.1
k_c	Exctinction coefficient due to phytoplankton Biomass	m^{-1}	0.03
ε_n	Remineralization rate for particulate nitrogen	d^{-1}	0.05
r_n	Ammonium oxidation rate by oxygen (nitrification)	d^{-1}	0.1
γ_{Zi}	Assimilation efficiency	unitless	0.7
W_{Dmax}	Sinking speed of the detritus material	m d^{-1}	10